ICSV14
Cairns • Australia
9-12 July, 2007

14th International Congress on Sound & Vibration

AN ASYMPTOTICALLY MOTIVATED HYRODYNAMIC-ACOUSTIC TWO-WAY COUPLING FOR MODELING THERMOACOUSTIC INSTABILITIES IN A RIJKE TUBE

Jonas P. Moeck[1]*, Heiko Schmidt[2], Michael Oevermann[3], Christian Oliver Paschereit[1], Rupert Klein[2]

[1]Institut für Strömungsmechanik und Technische Akustik
Technische Universität Berlin
10623 Berlin, Germany

[2]Fachbereich Mathematik/Informatik
Freie Universität Berlin
14195 Berlin, Germany

[3]Institut für Energietechnik
Technische Universität Berlin
10623 Berlin, Germany

jonas.moeck@pi.tu-berlin.de

Abstract

Thermoacoustic instabilities are a serious problem for lean premixed combustion systems. Due to different time and length scales associated with the flow field, combustion and acoustics, numerical computations of thermoacoustic phenomena are conceptionally challenging. Typically, the Mach numbers in gas turbine combustors are small. Nevertheless, numerical solvers are often based on compressible approaches in order to take into account the effect of the acoustic field. Considering the sensible interaction between chemical source terms and acoustics, spurious waves produced by these solvers may mislead the physical interpretation. For the low Mach number, long wave length case, we propose a bilateral coupling, where the region of heat release is described by a finite-difference zero Mach number solver. The larger acoustic domain is modeled by the common network approach for plane wave propagation. The coupling conditions are based on results from two-scale low Mach number asymptotics. As an example, simulation studies for a Rijke tube exhibiting self-excited oscillations are presented.

1. INTRODUCTION

Modern gas turbine technology relies on lean premixed combustion to satisfy stringent governmental emissions restrictions. Premixing the fuel with large quantities of air before injecting both into the combustor significantly reduces the peak temperatures and, thereby, leads to lower NOx emissions. The major drawback of this combustion mode is its high susceptibility to the excitation of high amplitude pressure pulsations commonly referred to as thermoacoustic instability. These self-excited oscillations result from the interaction of the unsteady heat release in the flame and the acoustic field of the combustor [1]. Negative effects of this phenomenon are increased noise, reduced system performance and structural fatigue. In fact, the occurrence of combustion instabilities usually requires a full engine shutdown and inhibits further operation at these conditions, since the pressure pulsations can rapidly cause structural failure [2].

Computational modeling of thermoacoustic processes in combustion chambers in order to predict unstable operating regimes and to develop and test control methods is, therefore, highly desirable. As shown recently, fully compressible reacting flow computations based on large-eddy simulations manage to accurately capture the essential thermoacoustic interaction mechanisms in realistic configurations and bear quantitative comparison with experimental data [3]. The computational effort is, however, still exceedingly high. Also, it is far from trivial to impose the proper acoustic boundary conditions, represented by frequency dependent impedances or reflection coefficients, in a compressible CFD simulation.

Various modeling approaches of lower complexity (and, therefore, less computational demand) have been proposed in the literature. So-called network models divide the thermoacoustic system under investigation in several elements, each being represented by acoustic frequency response functions for plane wave (and possibly azimuthal) modes [1]. Coupling of the acoustic field with the flame is incorporated by means of a flame transfer function/matrix. These type of models have shown to agree reasonably well with measured instability regimes and oscillation frequencies [1]. The major weakness of the network approach is that the flame dynamics still need to be determined by experiment or by CFD (see, e.g., [4, 5]). Also, taking into account nonlinearities in the thermoacoustic flame response is not straightforward. Accordingly, the prediction of the oscillation amplitude under unstable conditions or capturing inherently nonlinear phenomena as, e.g., hysteretic dependencies of the pulsation amplitude on system parameters (see Lieuwen & Zinn [6]), is difficult.

In this work, a method is proposed which takes advantage of the efficient acoustic modeling capabilities of the network approach, while, on the other hand, incorporating the thermoacoustic (linear *and* nonlinear) flame response by means of a detailed numerical computation. Details on the methods for representing the reactive flow and the acoustic field, as well as on the coupling procedure, are given in Sec. 2. In Sec. 3, the approach is applied to a simple Rijke tube with a laminar one-dimensional flame, exhibiting self-excited oscillations under certain conditions.

2. MODELING APPROACH

In the low Mach number, long wave length case, which is encountered in typical gas turbine combustors, acoustic perturbations act on a scale L much larger than the axial extent l of burner and flame (Fig. 1). Therefore, the effect of an acoustic wave on the burner flow reduces to a global acceleration of a quasi-incompressible medium in the limit of vanishing Mach number [7]. Conversely, the large scale acoustic field receives the heat release by the flame, which acts as a point source in-

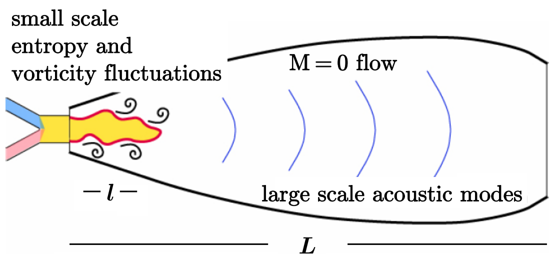

Figure 1. Scale separation between combustion/flow phenomena and long wave acoustics

ducing a jump in the velocity fluctuation. Our general strategy is to decouple the small scale hydrodynamic and the large scale acoustic computation. The bilateral coupling is achieved based on results from low Mach number asymptotics.

2.1. Small scale combustion

For the small scale part, we solve the variable density zero Mach number equations in one spatial dimension on a uniform grid. The balance equations for species mass fractions and temperature are

$$\rho \frac{\partial Y_s}{\partial t} + \rho u \frac{\partial Y_s}{\partial x} = -\frac{\partial j_s}{\partial x} + M_s \dot{\omega}_s, \tag{1}$$

$$\rho c_p \frac{\partial T}{\partial t} + \rho u c_p \frac{\partial T}{\partial x} = \frac{\mathrm{d}p}{\mathrm{d}t} - \frac{\partial q}{\partial x} - \sum_s j_s \frac{\partial h_s}{\partial x} - \sum_s h_s M_s \dot{\omega}_s, \tag{2}$$

with $s = 1, \ldots, n_s$. Here, ρ is the density, u the velocity, j_s the species diffusive flux, M_s the molecular weight of species s, $\dot{\omega}_s$ the chemical source term of species s, c_p the heat capacity at constant pressure, p the pressure, q the heat flux, and h_s the enthalpy of species s including the heats of formation. In the zero Mach number limit, the pressure is spatially constant and we have a divergence constraint on the velocity

$$\frac{\partial u}{\partial x} = -\frac{1}{\gamma\, p}\frac{\mathrm{d}p}{\mathrm{d}t} - \frac{1}{\rho c_p T}\left\{\frac{\partial q}{\partial x} + \sum_s j_s \frac{\partial h_s}{\partial x}\right\} - \frac{1}{\rho}\sum_s \left\{\frac{M}{M_s}\frac{\partial j_s}{\partial x}\right\} + \frac{1}{\rho}\sum_s \left\{\frac{M}{M_s} - \frac{h_s}{c_p T}\right\}\dot{\omega}_s. \tag{3}$$

The velocity at the inflow boundary is set equal to the time dependent flame speed. Integrating (3) over the whole domain from $x = x_1$ to $x = x_1 + l$ yields the velocity outflow condition. The density is calculated from the equation of state for an ideal gas $p = \rho T \sum_s Y_s R_s$.

The zero Mach number equations are solved numerically using a standard second-order finite-difference discretization. The time integration of the stiff set of equations is performed using the DAE solver IDA of the SUNDIALS package [8]. Thermodynamic and transport properties as well as reaction rates are calculated using the C++ interface of the CANTERA software package [9]. Diffusion velocities are computed using a mixture-based formulation with variable Lewis numbers for all species. A conservative multi-dimensional finite-volume presentation is discussed in Schmidt et al. [10].

2.2. Coupling based on low Mach number asymptotics

Klein [7] introduces an asymptotic multiple scale ansatz

$$\boldsymbol{U}(\boldsymbol{x}, t; \mathrm{M}) = \sum_i \mathrm{M}^i \boldsymbol{U}^{(i)}(\boldsymbol{x}, \mathrm{M}\boldsymbol{x}, t), \tag{4}$$

where he expands the solution vector $\boldsymbol{U} = (\rho, \boldsymbol{u}, T)^T$ in powers of the Mach number. Here, $\boldsymbol{x}$ resolves the short hydrodynamic length scale and $\xi = \mathrm{M}\boldsymbol{x}$ the acoustic scale. Three different physically relevant parts of the pressure are identified:

$$p(\boldsymbol{x}, t; \mathrm{M}) = \underbrace{P_0(t)}_{\text{thermodynamic}} + \underbrace{\mathrm{M}p^{(1)}(\mathrm{M}\boldsymbol{x}, t)}_{\text{acoustic}} + \underbrace{\mathrm{M}^2 p^{(2)}(\boldsymbol{x}, \mathrm{M}\boldsymbol{x}; t)}_{\text{hydrodynamic pressure part}}. \tag{5}$$

Inserting the ansatz (5) into Eq. (3), one observes that – in addition to the hydrodynamic pressure $p^{(2)}$ – the large scale acoustic gradient $\nabla_\xi p^{(1)}$ influences the flow field at leading order. In a general multi-dimensional setting, this time dependent term is provided by the acoustic solver. However, in our one-dimensional application, both terms will not have any effect on the reactive calculation but are important for studying instabilities associated with multi-dimensional effects. Here, the acoustic solver influences the hydrodynamics only via a model that relates the chemical composition at the inflow to the acoustic velocity field (see Sec. 3.1).

The feedback from the small scale to the large scale solver are: i) the jump in velocity imposed by the divergence constraint (3), and ii) the pressure difference $\Delta\left(\mathrm{M}p^{(1)} + \mathrm{M}^2 p^{(2)}\right)$ across the CFD domain. Note that the latter is not present in the one-dimensional case.

A schematic of the coupling approach is shown in Fig. 2. The representation of the large scale acoustic field is explained in the next section.

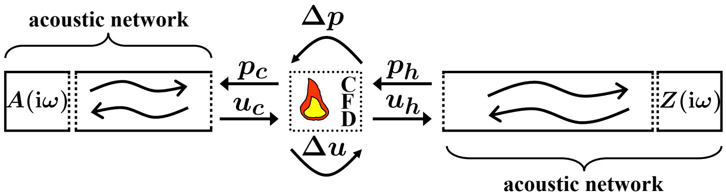

Figure 2. Schematic of the coupling approach

2.3. Large scale acoustics

For ease of notation, we consider p to be the acoustic pressure scaled by the characteristic impedance ρc in the following. With reference to the set-up shown in Fig. 2, the objective of the acoustic network model is to deliver time-domain relations for the lumped impedance downstream of the flame and the lumped admittance upstream of the flame. Eventually, these relations will take the form of finite dimensional linear time invariant systems, mapping p_l to u_l and u_r to p_r. The lumped impedance/admittance model contains all components affecting the plane wave response downstream/upstream of the flame. To obtain the lumped models, the advantages of the network approach can be exploited, i.e., individual elements can be characterized in a different way: by analytical considerations, system identification based on experimental data or finite element codes. Also, changing geometric parameters like duct lengths, etc., is easily accomplished.

When dealing with purely acoustic systems, a more intuitive approach is to model the input-output behavior of the plane wave mode in terms of the up- and downstream traveling waves, the so-called Riemann invariants g and f. In this case, we represent the generic acoustic element as a 2×2 mapping in standard state space form

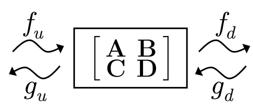

Figure 3. Generic aoustic element

$$\dot{\boldsymbol{x}} = \mathbf{A}\boldsymbol{x} + \mathbf{B}\begin{bmatrix} f_u \\ g_d \end{bmatrix}, \quad \begin{bmatrix} f_d \\ g_u \end{bmatrix} = \mathbf{C}\boldsymbol{x} + \mathbf{D}\begin{bmatrix} f_u \\ g_d \end{bmatrix}, \qquad (6)$$

where subscripts u and d denote up- and downstream positions. **A**, **B**, **C** and **D** are time-invariant $N\times N$, $N\times 2$, $2\times N$ and 2×2 matrices, respectively, and $\boldsymbol{x}$ is the N-dimensional state vector. With this approach, it was shown that the acoustic response of combustor like geometries can be modeled with high accuracy in frequency- and time-domain (see Paschereit et al. [11]).

Following this procedure, the combination of all acoustic elements downstream of the flame (say) yields a state space description of the reflection coefficient on the hot side,

$$\dot{\boldsymbol{x}} = \mathbf{A}\boldsymbol{x} + \mathbf{B} f_h, \qquad g_h = \mathbf{C}\boldsymbol{x} + D f_h, \tag{7}$$

where **B** and **C** are now length-N row and column vectors, respectively, and D is a scalar constant. The required relation mapping u_h to p_h is then written analogously as

$$\dot{\boldsymbol{x}} = \tilde{\mathbf{A}}\boldsymbol{x} + \tilde{\mathbf{B}} u_r, \qquad p_h = \tilde{\mathbf{C}}\boldsymbol{x} + \tilde{D} u_h. \tag{8}$$

It can be shown that the state space matrices in Eq. (8) are related to those in Eq. (7) by the transformation

$$\tilde{\mathbf{A}} = \mathbf{A} + \beta\mathbf{B}\mathbf{C}, \quad \tilde{\mathbf{B}} = \beta\mathbf{B}, \quad \tilde{\mathbf{C}} = 2\beta\mathbf{C}, \quad \tilde{D} = \beta(1 + D), \tag{9}$$

with $\beta = 1/(1 - D)$, and $D \neq 1$ has been assumed. Note, however, that in most of the cases, D will be zero. In fact, it is unlikely that the wave incident to the downstream part, f_h, has a direct feedthrough to the reflected wave g_h. A similar method, coupling state space representations of frequency dependent acoustic boundary conditions to a compressible CFD solver, was presented by Schuermans et al. [12].

3. APPLICATION TO A LAMINAR FLAME RIJKE-TUBE

3.1. Model set-up

Probably the simplest thermoacoustic system exhibiting self-excited oscillations generated by the interaction of unsteady heat release with the acoustic field is the well-known Rijke tube [13]. This device consists of a tube, usually with open-open or open-closed boundaries, with a heat source concentrated at a certain axial position. Heat is transferred to the fluid either by an electrically heated gauze [14] or by a compact flame (see, e.g., Morgans & Dowling [15]).

The set-up we consider here is an open-closed Rijke tube of constant cross-section with a laminar flame. Different tube lengths and degrees of acoustic reflectivity at the boundaries are used for the simulations. Methane is injected at a mean equivalence ratio of $\bar{\phi} = 0.7$ under constant pressure shortly before the flame front. In this case, we assume that acoustic velocity fluctuations induce perturbations in equivalence ratio via

$$\phi' = \bar{\phi}\left(\frac{1}{1 + k\,u'/\bar{u}} - 1\right), \tag{10}$$

as proposed by Peracchio & Proscia [16]. In Eq. (10), k accounts for mixing and kinematic dispersion (which we did not model) of the equivalence ratio fluctuations as they travel from the fuel injector to the flame front. For the simulation of the Rijke tube, k was set to 0.5. The axial extent of the domain represented by the flame code is 5 mm, the flame front being located at a distance of 1.5 mm (in the mean) from the upstream inlet. The flame dynamics were represented by a detailed reaction mechanism with 16 species, as given in Peters [17, p. 41]. Up- and downstream duct lengths, denoted by L_c and L_h, were chosen such that $L_h c_c/(L_c c_h) = 3/2$. Three different total lengths were considered, 2.8, 1.9 and 1.4 m.

According to the low Mach number Rankine-Hugoniot relations, continuity of pressure fluctuations is imposed at the flame front. Hence, in the special case of no pressure loss across the small scale combustion zone, the acoustic model has to provide for a time-domain relation that maps the velocity perturbations downstream of the flame to those upstream (see Fig. 2). This relation is obtained in the following way. The ducts up- and downstream of the flame are represented as time-delays for the wave amplitudes f and g. Truncation to a finite dimensional state space is then obtained by making use of Padé approximants. The resulting 2×2 input-output systems are connected to reflection coefficients of a given degree of reflectivity. This results in two relations of the form (7) for the hot and the cold side. Equation (9) is then employed to obtain a state space model for the hot side impedance. On the cold side, an analogous relation is used to represent the admittance, based on the reflection coefficient model. The output of the hot side impedance model is then connected to the cold side admittance. This yields the desired time-domain relation mapping u_h to u_c. To couple the acoustics to the flame code, this relation is represented as a discrete state-space model, viz.,

$$\boldsymbol{x}_{n+1} = \mathbf{A}\boldsymbol{x}_n + \mathbf{B}u_{h,n}, \qquad u_{c,n} = \mathbf{C}\boldsymbol{x}_n + Du_{h,n}, \tag{11}$$

with the same (fixed) time step that is used in the reacting flow simulation.

In the simple case of a duct with constant cross section, which we consider in this application, the corresponding frequency domain relation takes the form

$$\hat{u}_c = -\frac{(\rho c)_h}{(\rho c)_c}\,\frac{1+\mathrm{i}Z_c\tan(k_cL_c)}{Z_c+\mathrm{i}\tan(k_cL_c)}\,\frac{Z_h+\mathrm{i}\tan(k_hL_h)}{\mathrm{i}Z_h\tan(k_hL_h)+1}\,\hat{u}_h, \tag{12}$$

where $\hat{(\cdot)}$ denotes the Fourier transform, Z is the specific impedance, k denotes the wave number of the plane mode, $\mathrm{i} = \sqrt{-1}$, and subscripts h and c refer to conditions on the burned and unburned side, respectively. The frequency response of a typical discrete state space model (Eq. (11)) of order 26, as it is used in the coupled simulation, is plotted in Fig. 4 for the longest tube configuration with a boundary reflectivity of 0.8. The analytic relation (Eq. (12)) is added for comparison. Up to 600 Hz, the agreement is excellent. Deviations at higher frequencies are due to the Padé approximations used to represent the time-delays in state space. The accuracy in this frequency range could be increased by using higher order Padé approximants. However, since we consider only the long wave case, this representation was regarded as being sufficient.

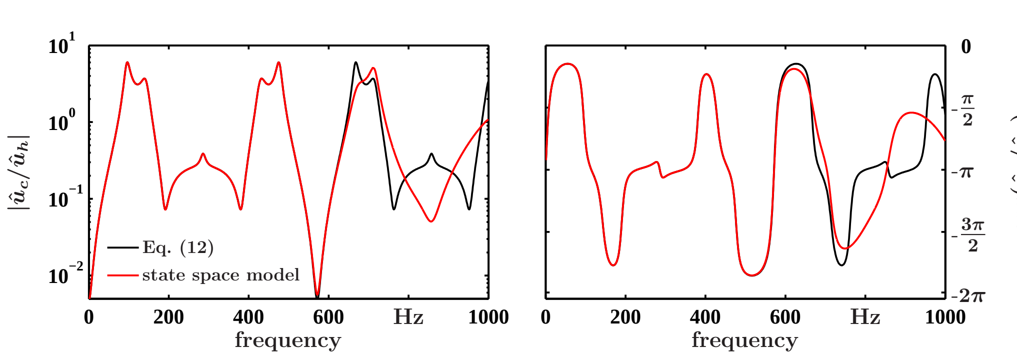

Figure 4. Frequency response relating velocity fluctuations downstream of the flame to those upstream

3.2. Simulation results

Coupled simulations were run for three different duct lengths with different degrees of reflectivity at the boundaries. The state vector in Eq. (11) was initialized with an array of uniformly distributed random numbers to favor the growth of unstable modes.

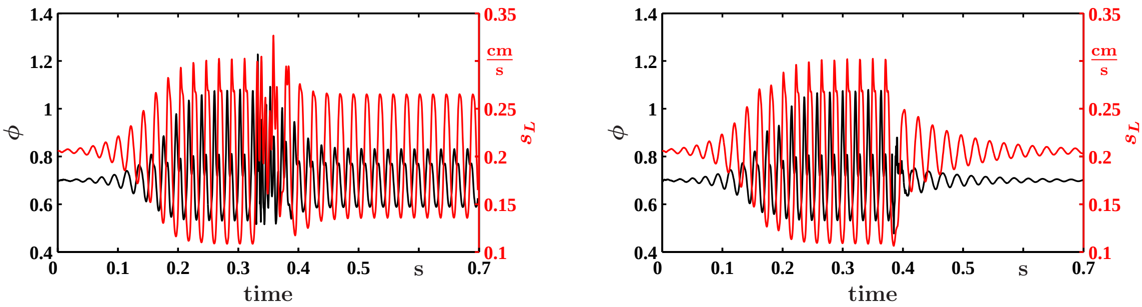

Figure 5. Time traces of equivalence ratio and laminar burning velocity for the longest tube with 2.8 m duct length. A finite amplitude limit cycle oscillation at 45 Hz is established. The reflection coefficient magnitude is decreased from 0.8 to 0.7 (left frame) and from 0.8 to 0.6 (right frame)

The left frame in Fig. 5 shows the temporal evolution of the laminar burning velocity, denoted by s_L, and the equivalence ratio for the case of the longest tube with 2.8 m duct length. At first, the reflection coefficient magnitude at the up- and downstream ends is set to 0.8. The system is unstable, and the quarter wave mode starts to grow until it settles on a finite amplitude limit cycle oscillation with a frequency of 45 Hz. At $t = 0.32$ s, the reflectivity of both boundary conditions is decreased to 0.7.

This results in a lower oscillation amplitude, however, the system is still unstable. In the right frame of Fig. 5, the results from the same computation are shown, except that now the reflectivity is decreased from 0.8 to 0.6 (at $t = 0.39$ s). This results in a stabilized system; the oscillations in equivalence ratio and burning velocity slowly decrease and settle to zero. If the reflectivity is reduced even further to 0.2, the system stabilizes almost immediately (Fig. 6) since virtually all fluctuation energy is lost at the boundaries.

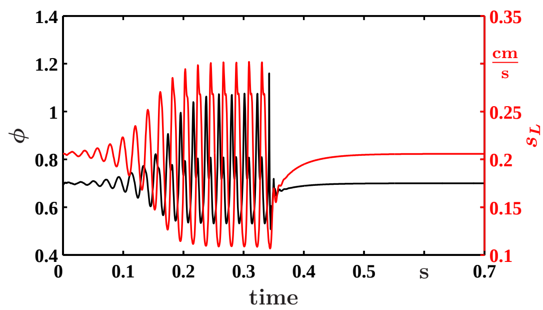

Figure 6. Time traces of equivalence ratio and laminar burning velocity. The reflection coefficient magnitude is decreased from 0.8 to 0.2

The temperature distribution in the combustion zone at three different times is presented in Fig. 7. At t_1, the oscillations are still small, so that the corresponding temperature profile represents the steady state case. The profiles labeled t_2 and t_3 are arbitrary snapshots on the limit cycle, illustrating the fluctuating temperature distribution induced by the equivalence ratio perturbations. This results in an oscillating net expansion across the combustion zone, imposed by the divergence constraint (Eq. (3)). The associated jump in the velocity perturbation further drives the acoustic field in the tube and compensates the energy loss at the boundaries due to imperfect reflection.

Additionally, simulations with shorter tubes were run. Figure 8 presents time traces of equivalence ratio and burning velocity for tubes with 2/3 (left frame) and 1/2 (right frame) of the initial length. The flame was kept at the same relative position, and the reflection coefficient magnitude at up- and downstream boundaries was set to 0.8. In both cases, the initial perturbations are damped out rapidly. However, a decaying oscillation at the mode frequencies can be observed. The reason for higher thermoacoustic stability in the case of shorter tubes is believed to result from less susceptibility of the flame to perturbations at higher frequencies, as was found in initial open-loop forcing studies. Therefore, the coupling of the heat release to higher mode frequencies, in case of shorter tubes, is less efficient, and the energy gain through the Rayleigh-integral does not exceed the losses at the boundaries.

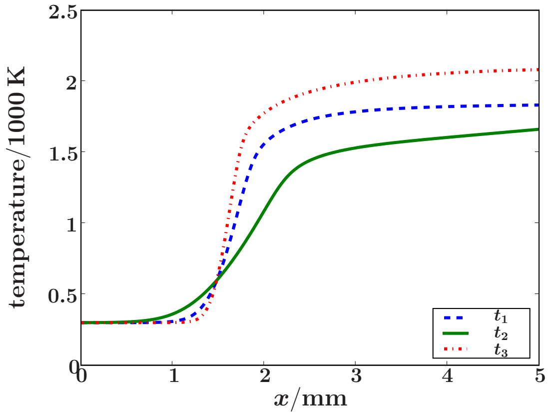

Figure 7. Temperature distribution in the combustion zone at three different times. Reflection coefficient magnitude set to 0.8

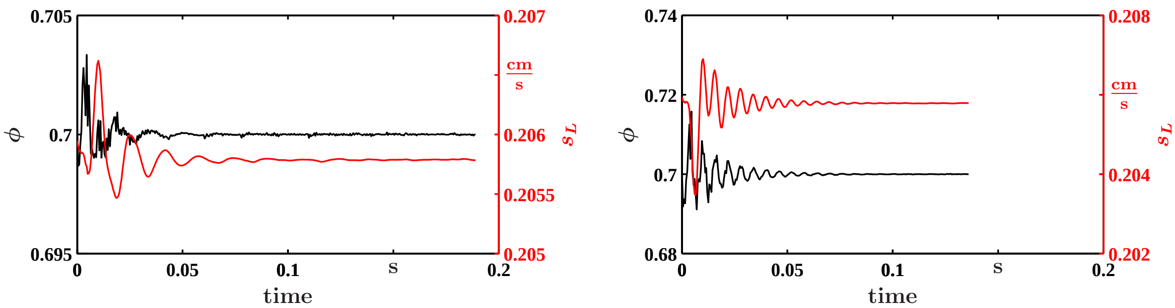

Figure 8. Time traces of equivalence ratio and laminar burning velocity. Tube length reduced by 1/3 (left frame) and by 1/2 (right frame)

4. CONCLUSIONS AND OUTLOOK

We presented a hybrid method for the simulation of thermoacoustic instabilities, exploiting the scale separation between small scale combustion phenomena and long wave acoustics. The approach was applied to a classical Rijke tube, exhibiting self-excited oscillations. In this configuration, we considered a laminar flame. The next step is to include turbulence effects, e.g., via one-dimensional turbulence models as proposed by Kerstein [18] and study the effect on thermoacoustic stability and the oscillation amplitude in case of unstable conditions. The Rijke tube was only a simple test case, but there is no principal difficulty to apply the proposed coupled method to more realistic configurations, e.g., to investigate the thermoacoustic characteristics of a swirl-stabilized combustor. While keeping the acoustic part of the solver, we currently exchange the one-dimensional laminar flame model against a three-dimensional turbulent flow solver that uses a flame capturing/tracking scheme.

The presented flame-acoustic coupling based on low Mach number asymptotics is certainly not more accurate than an approach based on fully compressible equations. However, it is clearly more efficient for two reasons: i) detailed numerical resolution is only applied where necessary (i.e., in the combustion zone); ii) computing costs are significantly reduced by using a zero Mach flow/combustion solver. Moreover, by using network techniques to model the long wave acoustics, it is straightforward to implement accurate frequency dependent boundary conditions – a component having an essential impact on pulsation amplitudes and stability characteristics of thermoacoustic systems. Due to the reduced complexity, this modeling approach is also suitable to develop and test control methodologies for the suppression of combustion instabilities.

ACKNOWLEDGEMENTS

Financial support from the German Science Foundation through the Collaborative Research Center 557 "Control of Complex Turbulent Shear Flows" is gratefully acknowledged.

REFERENCES

[1] LIEUWEN, T. C., AND YANG, V., eds., 2005. *Combustion Instabilities in Gas Turbine Engines*, Vol. 210 of *Progress in Astronautics and Aeronautics*. AIAA, Inc.

[2] SEWELL, J., SOBIESKI, P., AND BEERS, C., 2004. "Application of continuous combustion dynamics monitoring on large industrial gas turbines". ASME Paper GT2004-54310.

[3] SCHMITT, P., POINSOT, T., SCHUERMANS, B., AND GEIGLE, K. P., 2007. "Large-eddy simulation and experimental study of heat transfer, nitric oxide emissions and combustion instability in a swirled turbulent high-pressure burner". *J. Fluid Mech.,* **570**, pp. 17–46.

[4] SCHUERMANS, B., BELLUCCI, V., GUETHE, F., MEILI, F., FLOHR, P., AND PASCHEREIT, C. O., 2004. "A detailed analysis of thermoacoustic interaction mechanisms in a turbulent premixed flame". ASME Paper GT2004-53831.

[5] VAN KAMPEN, J. F., KOK, J. B. W., AND VAN DER MEER, T., 2007. "Efficient retrieval of the thermoacoustic flame transfer function from a linearized CFD simulation of a turbulent flame". *Int. J. Num. Meth. Fluids*. in press, doi: 10.1002/fld.1424.

[6] LIEUWEN, T. C., AND ZINN, B. T., 2000. "Experimental investigation of limit cycle oscillations in an unstable gas turbine combustor". AIAA Paper 2000-0707.

[7] KLEIN, R., 1995. "Semi-implicit extension of a Godunov type scheme based on low mach number asymptotics I: One-dimensional flow". *J. Comp. Phys.,* **121**, pp. 213–237.

[8] HINDMARSH, A. C., 2004. SUNDIALS: Suite of nonlinear and differential/algebraic equation solvers. Tech. Rep. UCRL-JRNL-200037, Lawrence Livermore National Laboratory.

[9] GOODWIN, D. CANTERA: Object-oriented software for reacting flows. http://www.cantera.org.

[10] SCHMIDT, H., OEVERMANN, M., MÜNCH, M., AND KLEIN, R., 2006. "Flame front capturing/tracking schemes for compressible and incompressible reactive flow". *Proc. ECCOMAS CFD Conf.*, Egmont aan Zee, The Netherlands.

[11] PASCHEREIT, C. O., MOECK, J. P., AND BOTHIEN, M. R., 2006. "State-space modeling of thermoacoustic systems for stability analysis and time domain simulation". *Proc. 13. Intl. Congr. Sound Vib.*, Vienna, Austria.

[12] SCHUERMANS, B., LUEBCKE, H., BAJUSZ, D., AND FLOHR, P., 2005. "Thermoacoustic analysis of gas turbine combustion systems using unsteady CFD". ASME Paper GT2005-68393.

[13] RAUN, R. L., BECKSTEAD, M. W., FINLINSON, J. C., AND BROOKS, K. P., 1993. "A review of Rijke tubes, Rijke burners and related devices". *Prog. Energy Combust. Sci.,* **19**(4), pp. 313–364.

[14] HECKL, M. A., 1990. "Non-linear Acoustic Effects in the Rijke Tube". *Acustica,* **72**, pp. 63–71.

[15] MORGANS, A. S., AND DOWLING, A. P., 2005. "Model-based control of a Rijke tube combustion instability". AIAA Paper 2005-2903.

[16] PERACCHIO, A. A., AND PROSCIA, W. M., 1999. "Nonlinear heat release/acoustic model for thermoacoustic instability in lean premixed combustors". *J. Eng. Gas Turb. Power,* **121**, pp. 415–421.

[17] PETERS, N., 1992. "Fifteen lectures on laminar and turbulent combustion". ERCOFTAC Summer School 1992, RWTH Aachen.

[18] KERSTEIN, A. R., 1989. "Linear-eddy modeling of turbulent transport. II: Application to shear layer mixing". *Combust. Flame,* **75**, pp. 397–413.